DOI: 10.1002/ejic.201100421

Organic Nanostructures with Controllable Morphology Fabricated from Ferrocene–Porphyrin Derivatives: Effect of Metal–Ligand Coordination on the Morphology, Dimensions, and Semiconductor Properties of Self-Assembled Nanostructures

Peihua Zhu,*[a,b] Pan Ma,[c] Yan Wang,[a] Quanbo Wang,[c] Xian Zhao,*[b] and Xiaomei Zhang*[c]

Keywords: Porphyrinoids / Sandwich complexes / Nanostructures / Self-assembly / Semiconductors

Two new ferrocene–porphyrin derivatives, namely 5,15-bis(ferrocenyl)-10,20-bis(4-nitrophenyl)porphyrin (**1**) and its nickel congener 5,15-bis(ferrocenyl)-10,20-bis(4-nitrophenyl)porphyrinatonickel (**2**) have been designed, synthesized, and characterized. Their self-assembly properties have been comparatively studied by electronic absorption and FTIR spectroscopy, TEM, SEM, XRD, and X-ray photoelectron spectroscopy (XPS). Metal-free **1** self-assembles into nanospheres with diameters in the range of 30–50 nm, depending mainly on intermolecular π–π interactions. In contrast, the coordination of nickel to **1** introduces an additional Ni–O coordination bond between the nitryl group of one molecule of **2** and the nickel center of the neighboring **2** unit, which, in cooperation with the intermolecular π–π interaction, induces the formation of nanobelts (ca. 50–300 μm length, 10–50 nm width) during the self-assembly process of **2**.

Introduction

Highly ordered nanostructures self-assembled from functional organic molecules have attracted extensive research interest for the purpose of constructing molecular-based electronic and optical devices such as electronic wires, switches, electroluminescent devices, field-effect transistors, and photovoltaic devices.[1,2] As a result, many organic nanostructures with elaborately designed molecules have been fabricated into nanofibres,[3] nanoribbons,[4] nanoparticles,[5] nanotubes,[6] and nanovesicles[7] in recent years.

As the one of the most important π conjugated systems, porphyrins have attracted interest due to their wide range of biologically relevant and industrial applications.[8] In recent years, the self-assembly behavior and nanostructures of porphyrin compounds have also started to attract interest.[9] Investigations have revealed that the self-assembly of porphyrin derivatives depends mainly on the intermolecular π–π interaction. However, introduction of different functional groups onto the peripheral positions of porphyrin molecules can induce additional intermolecular interactions, such as van der Waals, hydrogen bonding, hydrophilic/hydrophobic, electrostatic, and metal–ligand coordination. These factors, in cooperation and/or competition with the original π–π interaction between the porphyrin molecules, lead to the formation of nanostructures with different morphologies.[10] For example, an intermolecular π–π interaction of metal-free porphyrin $H_2[DP(CH_3COSC_5H_{10}O)_2P]$ leads to the formation of hollow nanospheres and nanoribbons in MeOH and *n*-hexane, respectively. In contrast, introduction of an additional Zn–O coordination bond in $Zn[DP(CH_3COSC_5H_{10}O)_2P]$ induces competition with the intermolecular π–π interaction, resulting in nanostructures with nanorod and hollow nanosphere morphologies in MeOH and *n*-hexane.[11] Synergistic interplay of the original π–π interaction with metal–ligand coordination or hydrogen bonding interactions has also been revealed to successfully tune the morphology of self-assembled nanostructures of porphyrin derivatives.[12]

For their unique physicochemical properties, ferrocenyl moieties have been introduced on to porphyrin rings using various strategies.[13] Ferrocene–porphyrins have emerged as efficient models for artificial photosynthesis owing to their ability to produce long-lived charge separated states and subsequent generation of a photocurrent.[14] These ferrocene–porphyrins contain multiredox-active centers, which is important for their application in molecular-based electronic devices[15] or molecular electrogenic sensors.[16]

[a] School of Chemistry and Chemical Engineering, University of Jinan,
Jinan 250022, China
E-mail: chm_zhuph@ujn.edu.cn
[b] State Key Laboratory of Crystal Material, Shandong University,
Jinan 250100, China
[c] Department of Chemistry, Shandong University,
Jinan 250100, China
Supporting information for this article is available on the WWW under http://dx.doi.org/10.1002/ejic.201100421.

Furthermore, the extremely rich electrochemical activity of ferrocene–porphyrins can be considered as an increased memory density allowing multibit information storage.

In this work, we describe the design and synthesis of two new ferrocene–porphyrin derivatives, namely 5,15-bis(ferrocenyl)-10,20-bis(4-nitrophenyl)porphyrin (**1**) and its nickel congener 5,15-bis(ferrocenyl)-10,20-bis(4-nitrophenyl)porphyrinatonickel (**2**). Their self-assembly has been investigated comparatively, revealing the effect of the Ni–O coordination bond on the morphology of self-assembled nanostructures. In addition, good semiconductor properties of the nanostructures fabricated from **1** and **2** have been revealed by *I*–*V* measurements.

Results and Discussion

Molecular Design, Synthesis, and Characterization

Highly ordered supramolecular structures are usually prepared by the self-assembly of porphyrin and phthalocyanine derivatives because of the dominant intermolecular π–π interaction between porphyrin and phthalocyanine molecules with large conjugated electronic structures. Meanwhile, the preferentially hexacoordinate nickel ion is introduced into the central hole of the porphyrin ligand, which is expected to provide an additional chance to tune the morphology and dimensions of aggregates based on the formation of metal–ligand coordination bonds. In addition, incorporating ferrocenyl units on to the peripheral positions of the porphyrin ring provides the possibility of fabricating nanoscale optoelectronic devices.

As shown in Scheme 1, **1** was synthesized in good yield from the condensation of ferrocenecarbaldehyde and 5-(4-nitrophenyl)dipyrromethane in the presence of $BF_3{\cdot}Et_2O$ in MeCN at 0 °C.[17,18] Its nickel congener **2** was obtained from the reaction of **1** and nickel acetate in DMF. Satisfactory elemental analyses were obtained for **1** and **2** after purification by column chromatography followed by repeated recrystallization from chloroform/methanol. The compounds were further characterized by MALDI-TOF mass spectrometry and ^1H NMR spectroscopy (Figures S1, S2, and S3, Supporting Information). The MALDI-TOF mass spectra of the compounds showed an intense signal for the protonated molecular ion $(M)^+$. The isotopic pattern closely resembled the simulation shown in Figure S1 (Supporting Information). These compounds were also characterized by electronic absorption and IR spectroscopy.

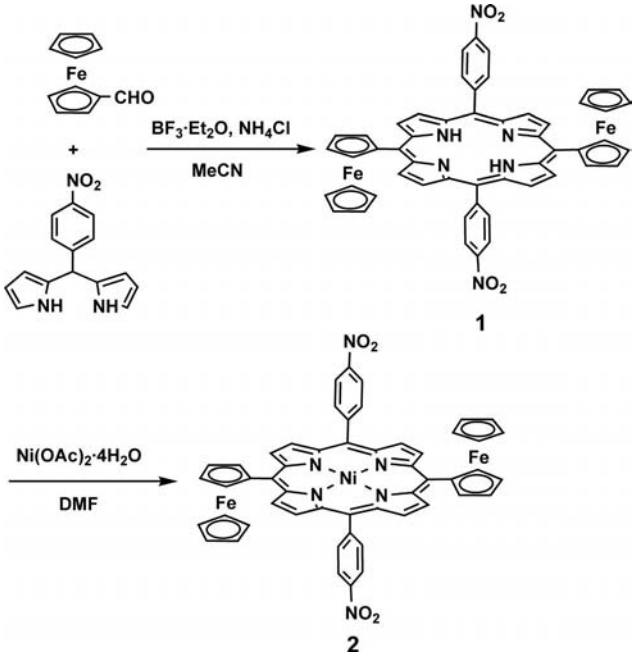

Scheme 1. Synthesis of **1** and **2**.

IR Spectra

The IR spectra of **1** and **2** and their self-assembled nanostructures formed in *n*-hexane are shown in Figures S4 and S5 (Supporting Information). The IR spectra of the nanostructures are similar to those of corresponding compounds, unambiguously confirming the composition of nanostructures from starting ferrocene–porphyrin compounds. Both **1** and **2** show an intense band at 1594 cm^{-1} due to N–O stretching vibrations.[19] A similar band is also observed at 1594 cm^{-1} in the IR spectrum of the self-assembled nanostructure fabricated from **1** in *n*-hexane (Figure S4). However, as can be seen in Figure S5, in the IR spectrum of the nanostructure fabricated from **2**, the N–O stretching vibration band is redshifted to 1489 cm^{-1}, indicating the formation of a Ni–O coordination bond between the oxygen atom of the nitryl attached to the *meso*-phenyl groups of **2** with the nickel ion of the neighboring **2** unit.

Electronic Absorption Spectra

The electronic absorption spectra of **1** and **2** were recorded in $CHCl_3$, and the data are compiled in Table S1 (Supporting Information). As seen in Figure 1, **1** and **2** showed typical features of metal-free and nickel–porphyrin compounds containing bis(ferrocenyl) moieties, respectively, revealing the nonaggregated nature of both in chloroform. The strong absorption peak with a maximum at 429 nm and three weak absorption peaks with maxima at 504, 637, and 704 nm for **1** can be attributed to the porphyrin Soret band and Q bands, respectively, (Figure 1, A) which is in line with that seen for 2,8,12,18-tetrabutyl-5,15-bis(ferrocenyl)-3,7,13,17-tetramethylporphyrin.[20] For **2**, the strong absorption peak with a maximum at 428 nm is attributed to its Soret band and the absorption peaks with maxima at 570 and 630 nm are attributed to its Q bands (Figure 1, B). It is worth noting that, compared to porphyrin derivatives without ferrocene moieties,[21] the Soret bands of these two compounds are broad, which is a remarkable feature for ferrocene–porphyrin compounds, and indicates the vibronic coupling between the porphyrin ring and the ferrocenyl moieties.[22]

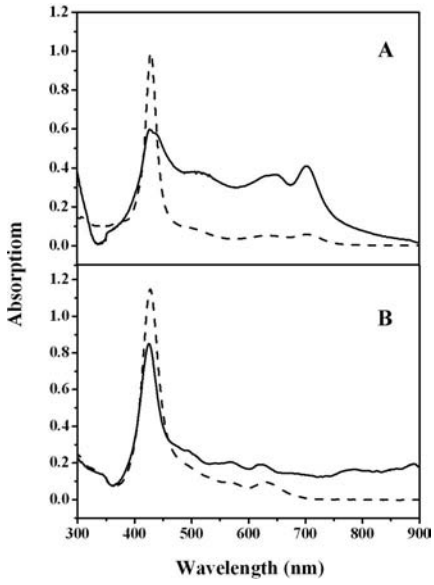

Figure 1. Electronic absorption spectra of **1** in dilute $CHCl_3$ solution (dashed line) and its self-assembled nanospheres dispersed in *n*-hexane (solid line) (A); compound **2** in dilute $CHCl_3$ solution (dashed line) and its self-assembled nanobelts dispersed in *n*-hexane (solid line) (B).

The electronic absorption spectra of the aggregates formed from **1** and **2** dispersed in *n*-hexane are also given in Figure 1. These are different from the spectra of the corresponding monomers in chloroform. As shown in part A of Figure 1, the porphyrin Q bands at 504 nm in $CHCl_3$ for **1** are redshifted to 512 nm when dispersed in *n*-hexane, and the porphyrin Soret band at 429 nm and the other Q bands seen at 637 and 704 nm in $CHCl_3$ remain almost unchanged. However, introduction of nickel induces blueshifts in all the porphyrin Soret and Q absorption bands for **2** from 428, 570, and 630 nm in $CHCl_3$ to 423, 569, and 626 nm in *n*-hexane, Figure 1 (B) and Table S1 (Supporting Information), indicating the effect of nickel on the molecular packing conformation in the aggregates due to the introduction of Ni–O bonding. On the basis of Kasha's exciton theory,[23] blueshifts in the main absorption bands of **2** upon aggregation reveal that the porphyrin molecules self-assemble into *H* aggregates with a face-to-face molecular arrangement in their nanostructures. In contrast, the redshifted absorption band in the electronic absorption spectra of **1** upon aggregation in *n*-hexane implies that the molecules of **1** are forced to adopt the *J* aggregation mode due to the steric hindrance of the two bulky bis(ferrocenyl) moieties. These results are in accord with the IR spectra, XRD, and XPS results.

Morphology of the Aggregates

The morphology of the aggregates was examined by TEM and SEM. Samples were prepared by casting a drop of the sample solution onto a carbon-coated grid. In line with the electronic absorption result, different morphologies were observed for the nanostructures formed from **1** and **2** (Figure 2). As shown in part A of Figure 2, molecules of **1** self-assembled in *n*-hexane uniformly into nanospheres with diameters in the range of 30–50 nm, depending mainly on π–π interactions between the porphyrin molecules. In contrast, molecules of **2** self-assembled uniformly into nanobelts, approximately 50–300 μm in length and 10–50 nm in width, due to the formation of a Ni–O coordination bond between the oxygen atom of the nitryl on the *meso*-phenyl groups of **2** with the nickel ion of the neighboring **2** molecule, Figure 2 (B and C). 1D nanobelts are believed to be ideal building blocks for nanoscale optoelectronic devices.[23] It is noteworthy that the distinct morphologies obtained from the self-assembly process of these two molecules clearly reflects the differences of intermolecular interactions, which induce different molecular packing conformations and morphologies. For **1**, the two bulky bis(ferrocenyl) moieties prevent effective stacking of the porphyrin molecules along one dimension to form 1D nanostructures. As a result, nanospheres were formed. However, introduction of nickel ions induces additional Ni–O coordination bonds between the oxygen atom of the nitryl on the *meso*-phenyl groups of **2** with the nickel ion of the neighboring molecule. This, in combination with the intermolecular π–π interactions, facilitates the linear stacking of **2**, which results in the formation of nanobelts.

X-ray Diffraction Patterns of the Aggregates

The internal structure of the self-assembled nanostructures of **1** and **2** was further investigated by XRD analysis. Figure 3 exhibits the diffraction patterns of the self-assembled nanostructures formed by **1** and **2**. As shown in Figure 3 (A), the XRD pattern of the nanospheres fabri-

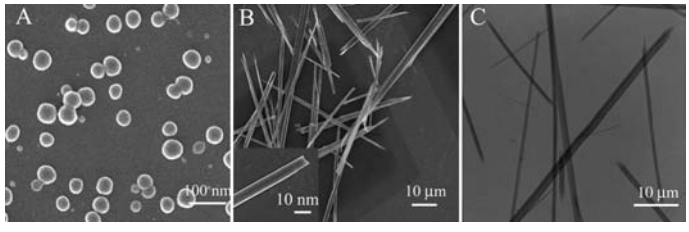

Figure 2. TEM and SEM images of self-assembled nanostructures of **1** and **2**. Nanospheres formed from **1** in *n*-hexane observed by SEM (A); Nanobelts formed from **2** in *n*-hexane observed by SEM (B) and TEM (C).

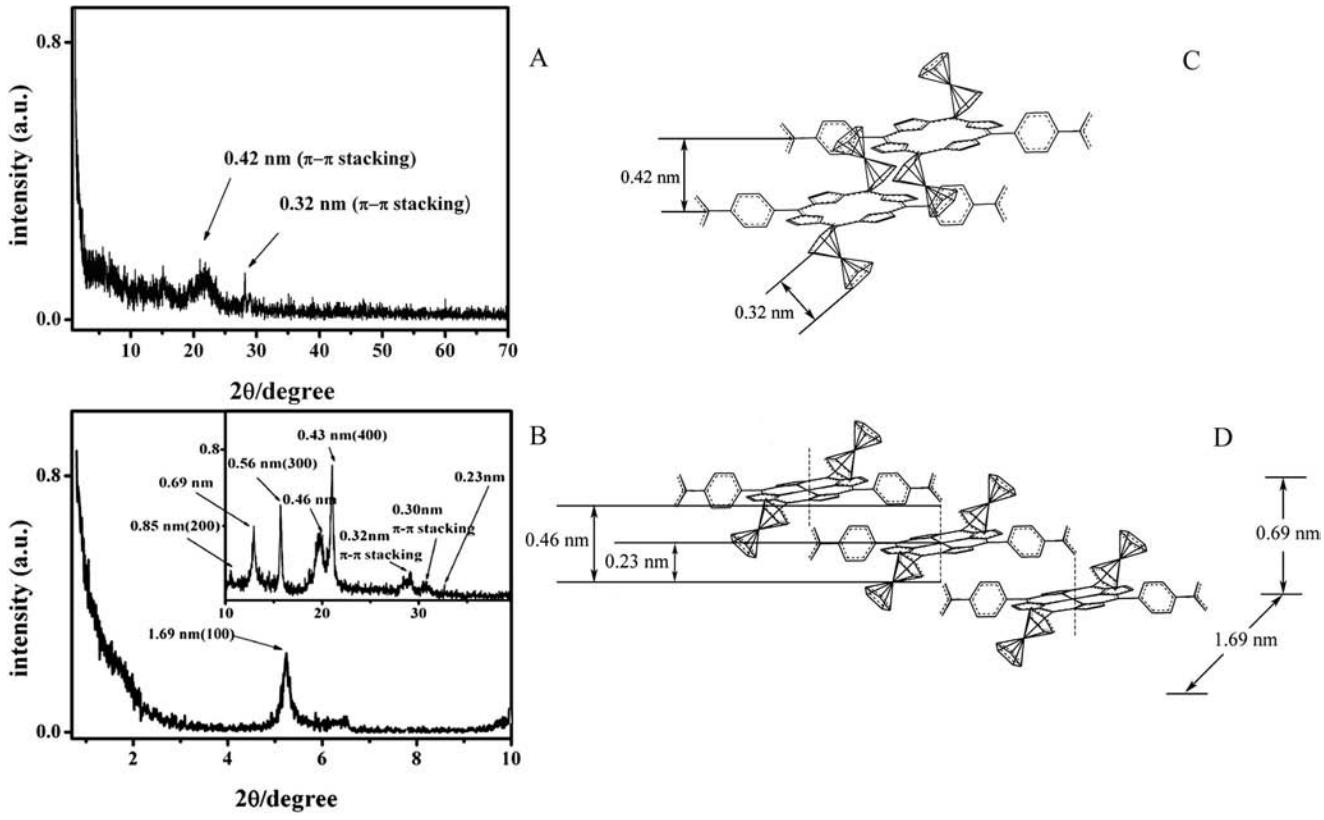

Figure 3. XRD profiles of the nanostructures of **1** (A) and **2** (B); schematic representations of the unit cells in the aggregates of **1** (C) and **2** (D).

cated from **1** shows one broad and one sharp peak at 2θ = 21.29 and 28.32° (corresponding to 0.42 and 0.32 nm), respectively. The broad band is ascribed to the stacking distance between neighboring porphyrin rings along the direction perpendicular to the porphyrin rings, in line with previous results (Figure 3, C).[25] The sharp band is attributed to the stacking distance between the cyclopentadiene cores of the ferrocenyl units along the direction perpendicular to the cyclopentadiene rings (Figure 3, C).[26]

As shown in Figure 3 (B), the XRD pattern of the nanobelts formed from **2** shows one narrow refraction peak at 2θ = 5.24° (corresponding to 1.69 nm) in the low angle range and a relatively weak peak at 2θ = 12.94° (corresponding to 0.69 nm) in the wide angle range, which are ascribed to the refraction from the (100) and (010) planes, respectively. The (100) plane also gives higher order refractions at 0.85 nm (200), 0.56 nm (300), and 0.43 nm (400) in the wide angle region of the XRD pattern. On the basis of the geometry optimization and the energy-minimized molecular structures of the ferrocene–porphyrins using the Gaussian 98 program at B3LYP/6-31G(d) level,[27] the width of **2** is ca. 1.69 nm. Therefore, the sharp peaks observed at 1.69 and 0.69 nm can be assigned to the width and height of a trimer of **2**, Figure 3 (D). Considering the average Ni–O coordination bond length of 0.23 nm, revealed by single-crystal XRD analysis,[28,29] the sharp peaks observed at 0.23 and 0.46 nm in the XRD pattern of the nanobelts formed from **2** can be assigned to the metal–ligand coordination bond length between the Ni and oxygen atoms and the two oxygen atoms coordinated to the central nickel ion above and below the porphyrin ring, respectively, as shown in Figure 3 (D). In addition, the nanobelts also present two refraction peaks at 0.30 and 0.32 nm in the wide angle region due to the stacking distance between the neighboring porphyrin rings[25] and the stacking distance between the cyclopentadiene cores of ferrocenyl units along the direction perpendicular to the cyclopentadiene rings, respectively.[25]

XPS Analysis

To confirm the existence of Ni–O coordination bonds between the nitryl oxygen attached to the *meso*-phenyl groups of the porphyrin molecule with the nickel center of the neighboring porphyrin molecule in the self-assembled nanobelts of **2**, XPS was employed to detect the nickel ion circumstances. Figure 4 displays the XPS spectra of **2** in chloroform and solid aggregates formed from **2**. As expected, both monomeric **2** and its self-assembled nanostructures show typical signals for the Ni^{2+} ion in their XPS spectra.[30] The strong absorption peak at 855.7 eV and the weak absorption peaks at 873.1 eV for monomeric **2** can be attributed to $Ni^{2+}{}_{2p3/2}$ and $Ni^{2+}{}_{2p1/2}$, respectively. However, the Ni^{2+} signals in the XPS spectra of the nanostructures are shifted to a lower bonding energy direction in compari-

son with monomeric **2** in chloroform, indicating a change of Ni^{2+} circumstances after the self-assembly process, confirming the rationality of the self-assembly mechanism discussed above.

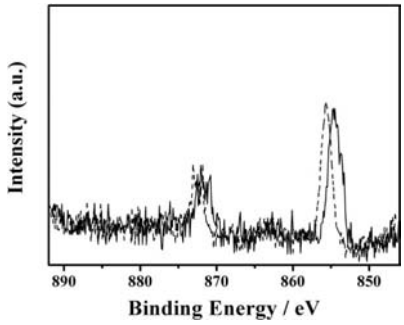

Figure 4. XPS spectra for **2** (dashed line) and aggregates of **2** (solid line) deposited on a silicon surface.

I–V Properties

To demonstrate the potential semiconductor properties of **1** and **2**, their nanostructures were carefully pressed onto two 0.24 mm spaced Au electrodes to measure their current–voltage characteristics. Figure 5 shows the current–voltage (*I–V*) characteristics of the nanostructures of **1** and **2**. For the devices measured, the conductivity for **1** and **2** extracted from the quasilinear region at low bias (up to 40 V) are about 7.51×10^{-7} and 3.39×10^{-6} $S\,m^{-1}$, respectively. The better semiconductor property of **2** might be due to its 1D π–π stacking structure and highly ordered crystalline molecular arrangement.

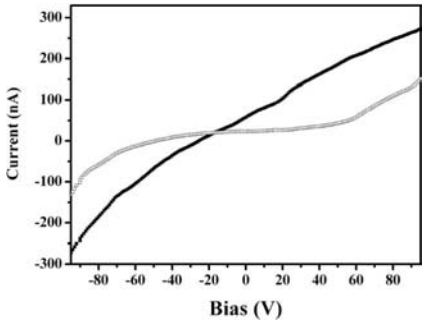

Figure 5. *I–V* curves measured on nanospheres formed from **1** (□) and nanobelts formed from **2** (■).

Conclusions

We have designed, synthesized, and investigated the self-assembly properties of ferrocene–porphyrin 5,15-bis(ferrocenyl)-10,20-bis(4-nitrophenyl)porphyrin (**1**) and its nickel congener 5,15-bis(ferrocenyl)-10,20-bis(4-nitrophenyl)porphyrinatonickel (**2**). Comparative investigation results reveal the effect of the Ni–O metal–ligand coordination bond on the molecular packing conformations and morphologies of the self-assembled nanostructures. Nevertheless, the nanobelts formed by **2** revealed better semiconductor properties with a conductivity of 3.39×10^{-6} $S\,m^{-1}$ than the nanospheres formed by **1** (7.51×10^{-7} $S\,m^{-1}$). These results not only reveal the effect of metal coordination bonds on the morphology of self-assembled nanostructures, but are also helpful in providing insight into the design and fabrication of nanostructures of porphyrin and phthalocyanine derivatives with good semiconductor properties.

Experimental Section

General: DMF was distilled from anhydrous $MgSO_4$ under reduced pressure prior to use. Column chromatography was carried out on silica gel (Merck, Kieselgel 60, 200–300 mesh) with the indicated eluent. All other reagents and solvents were of reagent grade and used as received. 5-(4-Nitrophenyl)dipyrromethane[31] and ferrocenecarbaldehyde[32] were prepared according to the published procedures.

Measurements: ^1H NMR spectra were recorded with a Bruker DPX 300 spectrometer (300 MHz) in $CDCl_3$ using the residual solvent resonance of $CHCl_3$ at δ = 7.26 ppm relative to $SiMe_4$ as internal reference. MALDI-TOF mass spectra were detected with a Bruker BIFLEX III ultra-high resolution Fourier transform ion cyclotron resonance (FT-ICR) mass spectrometer with α-cyano-4-hydroxycinnamic acid as matrix. Electronic absorption spectra were obtained with a Hitachi U-4100 spectrophotometer. Elemental analyses were performed with an Elementar Vavio El. FTIR spectra were recorded as KBr pellets with 2 cm^{-1} resolution using a αALPHA-T spectrometer. TEM images were obtained with a JEOL-100CX II electron microscope operated at 100 kV. SEM images were obtained with a JEOL JSM-6700F. For TEM imaging, a drop of sample solution was cast onto a carbon-coated copper grid. For SEM imaging, Au (1–2 nm) was sputtered onto the same grids to prevent charging effects and improve the image clarity.

Preparation of Nanoaggregates: The nanostructures of the porphyrin derivatives were fabricated by the solution mixture method according to the following procedure.[33] *n*-Hexane was injected rapidly into a solution of the porphyrin derivatives in chloroform (0.5 mM) to give a solution with final chloroform/*n*-hexane ratio of 1:3 (v/v) in a small flask. After the solution was allowed to equilibrate at ambient temperature for 2 d, loose aggregates were observed. These precipitates were then transferred to the carbon-coated grid by pipetting for TEM and SEM observations. The results were reproducible under the experimental conditions described above.

Device Fabrication: The nanostructures were obtained as films at the chloroform/*n*-hexane interface and transferred onto a SiO_2 substrate. After the solvent was evaporated, the Au electrodes were thermally evaporated onto the nanostructures by use of a shadow mask. These electrodes had a width of 28.6 mm and channel length of 0.24 mm. The current–voltage characteristics were obtained with a Keithley 4200 semiconductor characterization system at room temperature in air.

5,15-Bis(ferrocenyl)-10,20-bis(4-nitrophenyl)porphyrin (1): Ferrocenecarbaldehyde (856 mg, 4.0 mmol), 5-(4-nitrophenyl)dipyrromethane (1.06 g, 4.0 mmol), and NH_4Cl (2.14 g, 4.0 mmol) were dissolved in MeCN (400 mL) and $BF_3{\cdot}Et_2O$ (126 μL, 1.00 mmol) was added. The mixture was stirred at 0 °C under N_2 for 12 h. *p*-Chloranil (984 mg, 4.0 mmol) was added and the resultant solution was stirred for additional 4 h at room temperature. The reaction

mixture was chromatographed on an alumina column with $CHCl_3$ as eluent, and further purified by silica gel column chromatography. Recrystallization from $CHCl_3$/MeOH gave **1** (450 mg, 12.6%). ^1H NMR ($CDCl_3$, 300 MHz): δ = 9.88 (d, 4 H, Por β H), 8.66 (d, 4 H, Ph H), 8.57 (d, 4 H, Por β H), 8.37 (d, 4 H, Ph H), 5.51 (s, 4 H, Fc H), 4.86 (s, 4 H, Fc H), 4.13(s, 10 H, Fc H), –1.67 (s, 2 H, Por N H) ppm. MALDI-TOF MS: an isotopic cluster peaking at *m*/*z* 921.2; calcd. for $C_{52}H_{36}N_6O_4Fe_2$ $[M + H]^+$: 921.2. $C_{52}H_{36}Fe_2N_6O_4 \cdot 0.25CH_3OH$ (927.98): calcd. C 67.58, H 4.02, N 9.05; found C 67.13, H 3.91, N 8.98.

Preparation of 5,15-Bis(ferrocenyl)-10,20-bis(4-nitrophenyl)porphyrinatonickel(II) (2): A solution of **1** (37 mg, 40 μmol) was treated with a solution of $Ni(OAc)_2$ (424 mg, 1.6 mmol) in DMF (15 mL) and the mixture was stirred for 16 h. After metallation was complete (monitored by TLC), the reaction mixture was washed with water, dried with Na_2SO_4, concentrated, and chromatographed (silica, $CHCl_3$). Recrystallization from $CHCl_3$/MeOH gave purple solid (30 mg, 77%). ^1H NMR ($CDCl_3$, 300 MHz): δ = 9.58 (d, 4 H, Por β H), 8.56 (d, 4 H, Ph H), 8.49 (d, 4 H, Por β H), 8.15 (d, 4 H, Ph H), 5.11 (s, 4 H, Fc H), 4.72 (s, 4 H, Fc H), 3.98 (s, 10 H, Fc H) ppm. MALDI-TOF MS: an isotopic cluster peaking at *m*/*z* 975.8; calcd. for $C_{52}H_{34}N_6O_4Fe_2Ni$ $[M]^+$: 976.0. $C_{52}H_{34}Fe_2N_6NiO_4 \cdot 0.25CH_3OH$ (984.66): calcd. C 63.69, H 3.58, N 8.53; found C 63.26, H 3.56, N 8.40.

Supporting Information (see footnote on the first page of this article): Experimental and simulated isotopic pattern for the molecular ion of **2** shown in the MALDI-TOF mass spectrum. ^1H NMR spectra of **1** and **2** in $CDCl_3$ (* indicates solvent impurities). IR spectra of **1**, **2**, aggregates of **1** with nanosphere morphology, and aggregates of **2** with nanobelt morphology in the region 400–2500 cm^{-1} with 2 cm^{-1} resolution. TEM image of nanospheres formed from **1**. SEM images of the two-electrode device based nanospheres formed from **1** (A); nanobelts formed from **2** (B). Electronic absorption spectroscopic data for **1** and **2** dissolved in $CHCl_3$ and the self-assembled aggregates dispersed in *n*-hexane.

Acknowledgments

Financial support from the National Natural Science Foundation of China, the Postdoctoral Scientific Foundation of China and Shandong (grant No. 200903058) and the Doctoral Foundation of Shandong (grant No. 2007BS02016) is gratefully acknowledged.

[1] a) P. G. Schouten, J. M. Warman, M. P. de Haas, M. A. Fox, H. L. Pan, *Nature* **1991**, *353*, 736–737; b) J.-M. Lehn, *Science* **2002**, *295*, 2400–2403.

[2] a) J.-M. Lehn, *Supramolecular Chemistry, Concepts and Perspectives*, Wiley-VCH, New York, **1995**; b) S. Förster, T. Plantenberg, *Angew. Chem. Int. Ed.* **2002**, *41*, 688–714; c) J. J. L. M. Cornelissen, A. E. Rowan, R. J. M. Nolte, N. A. J. M. Sommerdijk, *Chem. Rev.* **2001**, *101*, 4039–4070; d) F. Tao, S. L. Bernasek, *Chem. Rev.* **2007**, *107*, 1408–1453; e) J.-H. Ryu, L. Tang, E. Lee, H.-J. Kim, M. Lee, *Chem. Eur. J.* **2008**, *14*, 871–881.

[3] a) M. Yun, N. V. Myung, R. P. Vasquez, C. Lee, E. Menke, R. M. Penner, *Nano Eur. J. Org. Chem. Lett.* **2004**, *4*, 419–422; b) H. Gan, H. Liu, Y. Li, Q. Zhao, Y. Li, S. Wang, T. Jiu, N. Wang, X. He, D. Yu, D. Zhu, *J. Am. Chem. Soc. Chem.* **2005**, *127*, 12452–12453.

[4] a) K. Balakrishnan, A. Datar, R. Oitker, H. Chen, J. Zuo, L. Zang, *J. Am. Chem. Soc. Chem.* **2005**, *127*, 10496–10497; b) K. Balakrishnan, A. Datar, T. Naddo, J. Huang, R. Oitker, M. Yen, J. Zhao, L. Zang, *J. Am. Chem. Soc. Chem.* **2006**, *128*, 7390–7398.

[5] X. Gong, T. Milic, C. Xu, J. D. Batteas, C. M. Drain, *J. Am. Chem. Soc. Chem.* **2002**, *124*, 14290–14291.

[6] a) J. M. Schnur, *Science* **1993**, *262*, 1669–1676; b) T. Shimizu, M. Masuda, H. Minamikawa, *Chem. Rev.* **2005**, *105*, 1401–1444; c) J. Hu, Y. Guo, H. Liang, L. Wan, L. Jiang, *J. Am. Chem. Soc.* **2005**, *127*, 17090–17095; d) M. Steinhart, R. B. Wehrspohn, U. Gösele, J. H. Wendorff, *Angew. Chem. Int. Ed.* **2004**, *43*, 1334–1344; e) Q. Liu, Y. Li, H. Liu, Y. Chen, X. Wang, Y. Zhang, X. Li, J. Jiang, *J. Phys. Chem. C* **2007**, *111*, 7298–7301.

[7] a) D. M. Vriezema, J. Hoogboom, K. Velonia, K. Takazawa, P. C. M. Christianen, J. C. Maan, A. E. Rowan, R. J. M. Nolte, *Angew. Chem. Int. Ed.* **2003**, *42*, 772–776; b) Y. Li, X. Li, H. Liu, S. Wang, H. Gan, J. Li, N. Wang, X. He, D. Zhu, *Angew. Chem. Int. Ed.* **2006**, *45*, 3639–3643.

[8] a) *The Porphyrin Handbook* (Eds.: K. M. Kadish, K. M. Smith, R. Guilard), Academic Press, San Diego, CA, **2000**, vol. 1–10; 2003, vol. 11–20; b) I. Hamza, *ACS Chem. Biol.* **2006**, *1*, 627–629; c) P.-C. Lo, C. M. H. Chan, J.-Y. Liu, W.-P. Fong, D. K. P. Ng, *J. Med. Chem.* **2007**, *50*, 2100–2107.

[9] a) C. M. Drain, A. Varotto, I. Radivojevic, *Chem. Rev.* **2009**, *109*, 1630–1658; b) H. Liu, J. Xu, Y. Li, Y. Li, *Acc. Chem. Res.* **2010**, *43*, 1496–1508; c) C. Huang, Y. Li, Y. Song, Y. Li, H. Liu, D. Zhu, *Adv. Mater.* **2010**, *22*, 3532–3536; d) C. Huang, L. Wen, H. Liu, Y. Li, X. Liu, M. Yuan, J. Zhai, L. Jiang, D. Zhu, *Adv. Mater.* **2009**, *21*, 1721–1725.

[10] a) M. Kimura, H. Narikawa, K. Ohta, K. Hanabusa, *Chem. Mater.* **2002**, *14*, 2711–2717; b) X. Huang, F. Zhao, Z. Li, Y. Tang, F. Zhang, C. Tung, *Langmuir* **2007**, *23*, 5167–5172; c) A. de la Escosura, M. V. M. Díaz, P. Thoedarson, A. E. Rowan, R. J. M. Nolte, T. Torres, *J. Am. Chem. Soc.* **2003**, *125*, 12300–12308; d) P. Chen, X. Ma, M. Liu, *Macromolecules* **2007**, *40*, 4780–4784.

[11] Y. Gao, X. Zhang, C. Ma, X. Li, J. Jiang, *J. Am. Chem. Soc.* **2008**, *130*, 17044–17052.

[12] G. Lu, X. Zhang, X. Cai, J. Jiang, *J. Mater. Chem.* **2009**, *19*, 2417–2424.

[13] C. Bucher, C. H. Devillers, J. C. Moutet, G. Royal, E. Saint-Aman, *Coord. Chem. Rev.* **2009**, *253*, 21–36.

[14] a) H. Imahori, Y. Sekiguchi, Y. Kashiwagi, T. Sato, Y. Araki, O. Ito, H. Yamada, S. Fukuzumi, *Chem. Eur. J.* **2004**, *10*, 3184–3196; b) M. U. Winters, E. Dahlstedt, H. E. Blades, C. J. Wilson, M. J. Frampton, H. L. Anderson, B. Albinsson, *J. Am. Chem. Soc.* **2007**, *129*, 4291–4297.

[15] a) J. R. Health, P. J. Kuekes, G. S. Snider, R. S. Williams, *Science* **1998**, *280*, 1716–1721; b) Y. Chen, J. Jung, D. Ohlberg, X. Li, D. R. Stewart, K. A. Jeppesen, J. F. Stoddart, R. S. Williams, *Nanotechnology* **2003**, *14*, 462–468.

[16] P. D. Beer, P. A. Gale, G. Z. Chen, *Coord. Chem. Rev.* **1999**, *185/186*, 3–36.

[17] a) J. P. Nagarkatti, K. R. Ashley, *Synthesis* **1974**, 186–187; b) B. J. Littler, Y. Ciringh, J. S. Lindsey, *J. Org. Chem.* **1999**, *64*, 2864–2872; c) D. M. Wallace, S. H. Leung, M. O. Senge, K. M. Smith, *J. Org. Chem.* **1993**, *58*, 7245–7257.

[18] J. K. Laha, S. Dhanalekshmi, M. Taniguchi, A. Ambroise, J. S. Lindsey, *Org. Process Res. Dev.* **2003**, *7*, 799–812.

[19] K.-L. Cheng, H.-W. Li, K. P. Ng. Dennis, *J. Organomet. Chem.* **2004**, *689*, 1593–1598.

[20] P. D. W. Boyd, A. K. Burrell, W. M. Campbell, P. A. Cocks, K. C. Gordon, G. B. Jameson, D. L. Officer, Z. Zhao, *Chem. Commun.* **1999**, 637–638.

[21] L. Pekkarinen, H. Linschitz, *J. Am. Chem. Soc.* **1960**, *82*, 2407–2411.

[22] V. S. Lin, S. G. DiMagno, M. J. Therien, *Science* **1994**, *264*, 1105–1111.

[23] a) A. Ulman, J. Manassen, *J. Am. Chem. Soc.* **1975**, *97*, 6540–6544; b) M. Kasha, H. R. Rawls, M. A. EI-Bayoumi, *Pure Appl. Chem.* **1965**, *11*, 371–392.

[24] M. Law, J. Goldberger, P. Yang, *Annu. Rev. Mater. Res.* **2004**, *34*, 83–122.

[25] a) J. Janczak, Y. M. Idemori, *Inorg. Chem.* **2002**, *41*, 5059–5065; b) A. S. Gardberg, S. Yang, B. M. Hoffman, J. A. Ibers, *Inorg. Chem.* **2002**, *41*, 1778–1781.
[26] a) P. D. W. Boyd, A. K. Burrell, W. M. Campbell, P. A. Cocks, K. C. Gordon, G. B. Jameson, D. L. Officer, Z. Zhao, *Chem. Commun.* **1999**, 637–638; b) S. W. Rhee, Y. H. Na, Y. Do, J. Kim, *Inorg. Chim. Acta* **2000**, *309*, 49–56.
[27] M. J. Frisch, G. W. Trucks; H. B. Schlegel, G. E. Scuseria, M. A. Robb, J. R. Cheeseman, J. A. Montgomery, T. Vreven Jr., K. N. Kudin, J. C. Burant, J. M. Millam, S. S. Iyengar, J. Tomasi, V. Barone, B. Mennucci, M. Cossi, G. Scalmani, N. Rega, G. A. Petersson, H. Nakatsuji, M. Hada, M. Ehara, K. Toyota, R. Fukuda, J. Hasegawa, M. Ishida, T. Nakajima, Y. Honda, O. Kitao, H. Nakai, M. Klene, X. Li, J. E. Knox, H. P. Hratchian, J. B. Cross, C. Adamo, J. Jaramillo, R. Gomperts, R. E. Stratmann, O. Yazyev, A. J. Austin, R. Cammi, C. Pomelli, J. W. Ochterski, P. Y. Ayala, K. Morokuma, G. A. Voth, P. Salvador, J. J. Dannenberg, V. G. Zakrzewski, S. Dapprich, A. D. Daniels, M. C. Strain, O. Farkas, D. K. Malick, A. D. Rabuck, K. Raghavachari, J. B. Foresman, J. V. Ortiz, Q. Cui, A. G. Baboul, S. Clifford, J. Cioslowski, B. B. Stefanov, G. Liu, A. Liashenko, P. Piskorz, I. Komaromi, R. L. Martin, D. J. Fox, T. Keith, M. A. Al-Laham, C. Y. Peng, A. Nanayakkara, M. Challacombe, P. M. W. Gill, B. Johnson, W. Chen, M. W. Wong, C. Gonzalez, J. A. Pople, *Gaussian 03*, revision B.05; Gaussian, Inc., Pittsburgh, PA, **2003**.
[28] J. A. R. Hartmann, S. P. Cooper, *Inorg. Chim. Acta* **1986**, *111*, L43–L46.
[29] a) M. P. Byrn, C. J. Curtis, I. Goldberg, Y. Hsiou, S. I. Khan, P. A. Sawin, S. K. Tendick, C. E. Strouse, *J. Am. Chem. Soc.* **1991**, *113*, 6549–6557; b) M. O. Senge, K. M. Smith, *J. Chem. Soc., Chem. Commun.* **1994**, 923–924; c) S. Adilov, V. R. Thalladi, *Cryst. Growth Des.* **2007**, *7*, 481–484.
[30] H. Winnischofer, T. C. R. Rocha, W. C. Nunes, L. M. Socolovsky, M. Knobel, D. Zanchet, *ACS Nano* **2008**, *2*, 1313–1319.
[31] B. J. Littler, M. A. Miller, C.-H. Hung, R. W. Wagner, D. F. O'Shea, P. D. Boyle, J. S. Lindsey, *J. Org. Chem.* **1999**, *64*, 1391–1396.
[32] M. Sato, H. Kono, M. Shiga, I. Motoyama, K. Hata, *Bull. Chem. Soc. Jpn.* **1968**, *41*, 252.
[33] a) K. Balakrishnan, A. Datar, T. Naddo, J. Huang, R. Oitker, M. Yen, J. Zhao, L. Zang, *J. Am. Chem. Soc.* **2006**, *128*, 7390–7398; b) W. Su, Y. Zhang, C. Zhao, X. Li, J. Jiang, *ChemPhysChem* **2007**, *8*, 1857–1862; c) X. Gong, T. Milic, C. Xu, J. D. Batteas, C. M. Drain, *J. Am. Chem. Soc.* **2002**, *124*, 14290–14291.

Received: April 19, 2011
Published Online: August 9, 2011

